Experimental study of viscous effects on flow pattern and bubble behavior in small diameter bubble column

Olumayowa T. Kajero, Mukhtar Abdulkadir, Lokman Abdulkareem, and Barry James Azzopardi

Citation: Physics of Fluids **30**, 093101 (2018); doi: 10.1063/1.5045160
View online: https://doi.org/10.1063/1.5045160
View Table of Contents: http://aip.scitation.org/toc/phf/30/9
Published by the American Institute of Physics

Experimental study of viscous effects on flow pattern and bubble behavior in small diameter bubble column

Olumayowa T. Kajero,[1,a)] Mukhtar Abdulkadir,[2] Lokman Abdulkareem,[3] and Barry James Azzopardi[4]
[1]*Department of Chemical and Process Engineering, University of Surrey, Guildford GU2 7XH, Surrey, United Kingdom*
[2]*Department of Chemical Engineering, Federal University of Technology, PMB 65 Minna, Nigeria*
[3]*Department of Petroleum Engineering, University of Zakho, P.O. Box 12, Zakho City, Northern Iraq*
[4]*Department of Chemical and Environmental Engineering, University of Nottingham, University Park, Nottingham NG7 2RD, United Kingdom*

(Received 18 June 2018; accepted 16 August 2018; published online 7 September 2018)

An experimental study was carried out to explore viscous effects on the flow pattern and bubble behavior in a small diameter bubble column using silicone oil fluids of viscosities 5, 100, 1000, and 5000 mPa s. The flow pattern was obtained from the probability density function using the time-averaged void fraction traces of the real-time qualitative and quantitative measurements from Electrical Capacitance Tomography (ECT). This was confirmed from the high-speed camera and ECT images which also gave a vivid description of the bubble behavior. Further confirmation of the observed flow pattern was obtained using the diameter ratio, λ, where for slug flow $\lambda > 0.6$. The flow pattern was observed to vary from spherical cap bubbles to developing slug and slug flow within the gas superficial velocities considered ($0.02 \leq U_{gs} \leq 0.361$ m/s). As viscosity increases, the appearance of spherical cap bubbles decreases, while slug flow tendency increases. The observed flow patterns were compared with previous work. The developing slugs in liquid viscosities of 5 and 100 mPa s were observed to be deformed. The Taylor bubble obtained from 1000 mPa s is called prolate spheroid, while that obtained from 5000 mPa s is called oblate spheroid. In addition, as the superficial gas velocity increases, the length of Taylor bubbles increases, while that of slug flow decreases. The bubble behavior was further characterised using the inverse dimensionless viscosity and Eotovos number. The process of leading and trailing bubble merging to form Taylor bubbles via coalescence was also captured and explained using the high-speed camera video. *Published by AIP Publishing.* https://doi.org/10.1063/1.5045160

I. INTRODUCTION

Gas-liquid two phase flow phenomena are of vital importance in many process industries involving the use of bubble column reactors. The flow characterization is generally dependent on flow patterns and bubble behavior. The flow pattern is influenced by the gas and liquid flow rate, gas pressure, fluid properties, direction of flow, orifice or nozzle diameter, dimensions of pipe or column, viscosity, etc. (Medjiade *et al.*, 2017). The effect of liquid viscosity on the flow pattern and bubble behavior has been considered by some researchers but not within a wide range of viscosities, as studied in this work.

Four main types of flow regimes have been observed in bubble column reactors. These include bubbly, slug, churn, and annular flow (Shaikh and Al-Dahhan, 2007 and Medjiade *et al.*, 2017), as shown in Fig. 1.

In bubbly flow, there is a continuous liquid phase and a gas phase with the latter dispersed as bubbles throughout the liquid. In slug flow, there is the formation of bullet shaped Taylor bubbles, with a thin film of liquid surrounding the bubbles, while in between the Taylor bubbles are liquid slugs which often contains a dispersion of smaller bubbles. Churn flow, characterised by strong intermittency and intense mixing, occurs at higher velocities, with the Taylor bubbles breaking down into churning or oscillatory motion. In annular flow, gas flows in the core of the column with an annulus of liquid flowing up the wall (Shaikh and Al-Dahhan, 2007 and Medjiade *et al.*, 2017).

The Taylor bubble is peculiar to slug flow where the large pockets of bullet shaped bubbles occupy almost the entire cross section of the tube or column. The Taylor bubble length has been described to exceed 1.5 times of the tube diameter or its diameter is greater than 60% of the tube diameter (Mandal *et al.*, 2007). The Taylor bubble contains a significant volume fraction of gas called the void fraction. This void fraction in Taylor bubbles is defined as the ratio of the area of gas in the Taylor bubble to that of the area of column containing gas and liquid. It is the fraction of gas in the Taylor bubble. The shape of the bubble has also been described to be prolate spheroid, when the nose has a spherical or curved front and a flat back due to the inertia controlling regime, and oblate spheroid when both the front and back of the bubble is spherical which is due to the viscous controlling regime (Fabre and Line, 1992 and Kajero *et al.*, 2012).

Weisman *et al.* (1979) investigated the effect of fluid properties and pipe diameter on two-phase flow patterns behavior

a)Author to whom correspondence should be addressed: m10767@surrey.ac.uk and ot.kajero@gmail.com

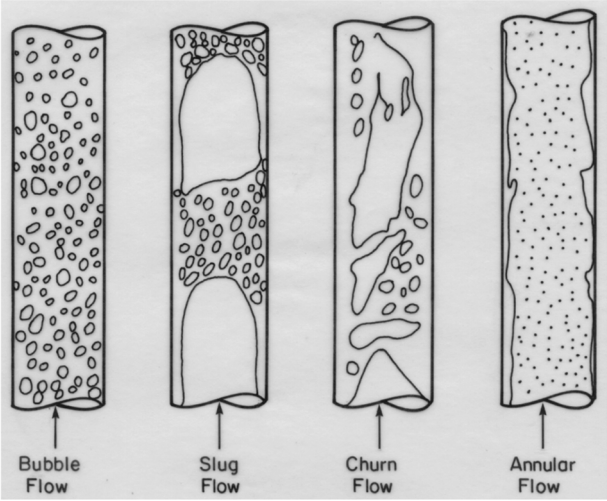

FIG. 1. Flow regimes in bubble column reactors. Reproduced with permission from Shaikh and Al-Dahhan, "A review on flow regime transition in bubble columns," Int. J. Chem. React. Eng. **5**, 1542 (2007), Review R1.4. Copyright 2007 Berkeley Electronic Press.

in horizontal pipes using air-glycerol water solutions with viscosities of 0.07 and 0.15 Pa s. They laid emphasis on the fact that flow patterns in vertical upward flow is strongly dependent on liquid viscosity (Hiroaki and Kiyoshi, 2011). Bousman *et al.* (1996) among other studies looked at the effect of liquid viscosity on flow patterns in microgravity using water (viscosity, 1 cP), water/glycerine (viscosity, 6 cP), and water/Zonyl FSP (viscosity, 1 cP). Changes in liquid viscosities affected the transition from bubbles to slug flow but not quite significant in the transition from slug to annular.

Furukawa and Fukano (2001) experimentally investigated the effect of liquid viscosity on flow patterns in vertical upward gas-liquid two-phase flow. They used a 19.2 mm diameter and 5.4 m long vertical tube with water (viscosity, 1 mPa s) and aqueous glycerol solutions (with viscosities 5.7 and 14.7 mPa s). Using visual and video observations, and still photography, alongside with a time-spatial characteristic map of interfaces (Furukawa, 1995), the flow patterns observed include bubble flow, bubble-slug flow, slug flow, slug-froth flow, froth flow, froth-annular flow, and annular flow. The changes in flow patterns due to variation in viscosities (1–1060 mPa s) of aqueous glycerol solution were studied by Keska *et al.* (2011) in a vertical pipe. The flow patterns observed were bubbly, slug, churn, annular, and mist.

Numerical simulation studies to explore bubble collapse have been carried out by Apazidis (2016), Koukouvinis *et al.* (2016a), and Koukouvinis *et al.* (2016b), while Cui *et al.* (2016) and Dabiri and Bhuvankar (2016) studied the coalescence of bubbles experimentally and numerically, respectively.

Cui *et al.* (2016) experimentally studied the interaction and coalescence of synchronized multiple bubbles. In the study, low-voltage electric discharges were used to generate the bubbles in a 0.5 m side cubic glass tank filled with water degassed by boiling. High-speed camera bubble images were obtained to study the bubble dynamics. The images revealed the interaction between two synchronized bubbles within the tank and the behavior of a bubble near the wall; the interaction of three synchronized bubbles at a collinearly equal dimensionless inter-bubbly distance; the interaction of three synchronized bubbles at an equal dimensionless inter-bubble distance; and the interaction of four synchronized bubbles at two given dimensionless inter-bubble distances.

Dabiri and Bhuvankar (2016) numerically studied the fluid dynamics of rising bubbles close to the wall in a vertical channel in the presence of upward flow parallel to the wall. The computations within the domain are based on the front-tracking/finite volume method. The bubble and liquid rise velocities were computed for different void fractions, Archimedes numbers, and Eotovos numbers, Eo. For small Eo, the bubbles are nearly spherical.

Apazidis (2016) simulated shock wave propagation in a water-filled circular cross-section tube by placing a spherical air bubble symmetrically at the tube axis. Different stages of bubble collapse were identified, one of which was the bubble breaking into two elongated regions, with the shock collapse of the second bubble strongly affected by the other. Using the Volume of Fluid (VOF) method, Koukouvinis *et al.* (2016a) simulated the collapse of bubbles in a water container with dimensions 178.2 mm × 178.2 mm × 190.2 mm. The simulation was 2D-axisymmetric which captures the process of bubble growth, collapse, and rebound. There was a significant expansion of the bubbles to form pressure waves that radiates in a spherical manner at all directions. The collapse of the bubbles commences after maximum bubble size was reached with subsequent formation of a deformed, non-spherical bubble. Similarly, Koukouvinis *et al.* (2016a) used the VOF method to simulate bubble flow in a 2D rectangular domain corresponding to the 178.2 mm diameter. The studies reveal the bubble expansion and collapse process, formation of tension waves, shape and breaking of bubbles, mushroom-shaped tip bubbles, and likewise corona formation.

Furthermore, Shen *et al.* (2017) studied the gas-liquid flow from a micro-channel using a wide range of gas and liquid viscosities. Clean air was bubbled through pure water into two ends of a horizontal tube with an inlet to a vertical microchannel with a diameter of 1.5 mm. Flow behaviors were captured with a high-speed CCD camera. The flow regimes identified were periodic bubbling, characterised by discrete bubbles which were spherical in shape and aperiodic bubbling bubbles, due to increasing velocity during which bubble formation loses its periodicity with coalescence taking place on multiple notes, i.e., double, triple, quadruple, and quintuple bubble formations. The flow regime transitions were classified into bubble, bubble-train Taylor, Taylor-annular, and Churn, with Taylor bubbles further classified into regular and irregular.

Sharaf *et al.* (2017) investigated the shapes and paths of an air bubble rising in quiescent liquids. They utilised an acrylic tank with dimensions 200 mm × 200 mm × 700 mm containing different viscosities of glycerol in water solution. The viscosity varies from 4.3 to 1657 mPa s. A high-speed camera was used to visualize the bubble flow, while Computational Fluid Dynamics (CFD) was used to simulate the dynamics of the rising air bubble with the observation of spherical, oblate, and dimpled bubbles. Medjiade *et al.* (2017) studied

experimentally the flow regimes in the bubble column with a diameter of 102 mm. They used the tap water/nitrogen system with the viscosities varied up to 16 mPa s. They observed that the bubbly region disappears with an increase in viscosity. A majority of the studies in bubble columns focus on large diameters with a small range of viscosities, hence the motivation behind this study (Nedeltchev and Shaikh, 2013; Azzopardi *et al.*, 2014; Nedeltchev, 2015; Nedeltchev and Schubert, 2015; and Medjiade *et al.*, 2017). In addition, both qualitative and quantitative real-time measurements were implemented in this study for the wide range of viscosities considered.

In this work, flow patterns and bubble behavior in 5, 100, 1000, and 5000 mPa s silicone oil have been studied in a 50 mm diameter and 1.6 m long Perspex column through the analysis of the data from Electrical Capacitance Tomography (ECT) to obtain the probability density function (PDF), an objective and quantitative approach, from which the flow pattern is obtained. This is compared with the video taken from the high-speed camera which also clearly depicts the flow pattern in comparison to the PDF and the bubble behavior. It was observed to vary from spherical cap bubbles to developing slug (deformed Taylor bubbles) and slug flow (developed Taylor bubbles). These have been related to the void fraction increase over the wide range of liquid viscosities considered due to the wall effect, drag force, and surface tension effect. In addition, the diameter ratio criteria according to Clift *et al.* (2005) and dimensionless parameters were also used to characterize the flow pattern. This is explained in detail in this paper.

II. FLOW PATTERN IDENTIFICATION

Several methods have been described for flow pattern identification. These includes flow visualization or visual observation (Taitel *et al.*, 1980), void fraction fluctuation from the radiation technique (Jones and Zuber, 1975), impedance technique (Merilo *et al.*, 1977), or pressure fluctuation (Tutu, 1982 and Matsui, 1984), Probability Density Function (PDF), further modification of the PDF into neural network (Mi *et al.*, 2001), and the use of the Chaos analysis (Lee *et al.*, 2008).

In this work, a flow pattern was obtained using:

i. visual observation monitored via the high-speed video camera images;
ii. Probability Density Function (PDF), using the time-averaged void fraction traces from the ECT and likewise, real-time ECT image displays; and
iii. the diameter ratio according to Clift *et al.* (2005), where the diameter ratio is given to be greater than 0.6 for slug, since a domineering flow pattern for the viscosities considered coupled with the column diameter used (50 mm) is slug flow.

A. Visual observation

Gas-liquid flow patterns and bubble behavior can be obtained via visualization through the naked eye and the capturing of the video using a high-speed camera. The video captured can be played to visually observe the displayed flow pattern and the bubble behavior.

In this work, the Phantom high-speed camera version 606 was used. Further analyses were carried out via the camera control software, which provides features through which the captured videos or images can be studied and analyzed.

B. Probability Density Function (PDF)

This is a statistical tool which can be used to identify the flow pattern. If we define a function $P(x)dx$ in which the data $x(t)$ lie on the value between x and $x + dx$, we have

$$P(x)dx = P(x < x(t) \leq x + dx). \tag{1}$$

The total area enclosed by this function must equal unity,

$$P(-\infty < x\infty) = \int_{-\infty}^{\infty} P(x)dx \equiv 1. \tag{2}$$

In terms of void fraction, the probability density function can be said to be the rate of change of the probability that void fraction lies within a certain range versus void fraction (Omeberi-Iyari and Azzopardi, 2007).

Flow pattern identification using the probability density function of void fraction as proposed by Jones and Zuber (1975) is summarized in Fig. 2. In their work, the photon attenuation technique was used to measure the time-varying cross-sectional void fraction, with the aid of a dual X-ray beam device for a vertical air-water two-phase flow mixture.

According to Costigan and Whalley (1997), discrete bubble flow has PDF trace with narrow single peaks and low void fraction; the spherical cap bubble has PDF trace with a long single peak of low void fraction (bubble flow) and a broadening tail of short or negligible peak extending to higher void fractions, while slug flow has two peaks with the high void fraction peak for Taylor bubbles and the low void fraction peak for liquid slugs.

The PDF for various liquid viscosities at different gas superficial velocities were obtained from the void fraction traces based on qualitative and quantitative real-time measurements from the ECT. In addition, the ECT provided real-time images of the flow pattern and bubble behavior within the flow domain.

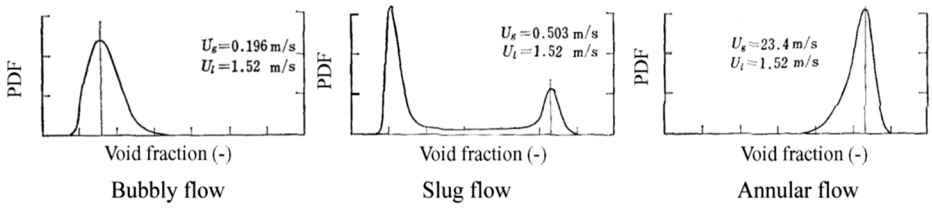

FIG. 2. Flow pattern identification proposed by Jones and Zuber (1975) using the probability density function of void fraction (Abdulkadir, 2011).

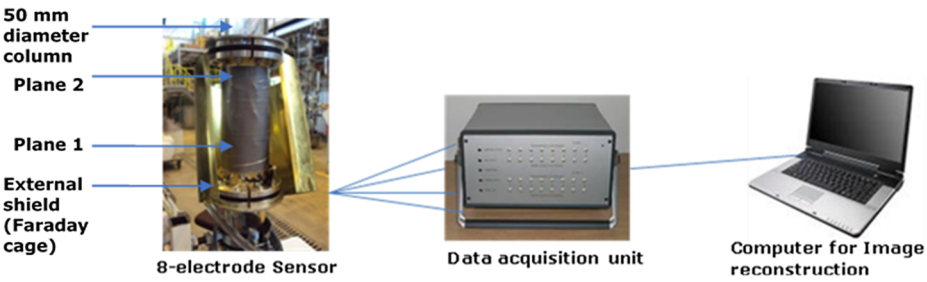

FIG. 3. The 50 mm diameter column having an ECT sensor with 8 electrodes.

C. Flow pattern confirmation using the diameter ratio, λ

The diameter ratio, λ, defined as the ratio of diameter of the bubble to that of the column can also be used to determine the flow pattern (Clift *et al.*, 2005). It is expressed as

$$\lambda = \frac{d}{D}. \tag{3}$$

The criteria used to determine the flow pattern are given as follows:

1. When the diameter ratio, λ, is less than 0.6, the flow pattern should be a spherical cap bubble (Hosoda *et al.*, 2011).
2. When the diameter ratio, λ, is greater than 0.6, the flow pattern should be slug flow (Clift *et al.*, 2005; Hosoda *et al.*, 2011; Wallis, 1969; Zukoski, 1966; and Tomiyama *et al.*, 2003).

III. EXPERIMENTAL ARRANGEMENTS

The experimental setup consists of a bubble column with 50 mm internal diameter and a height of 1.6 m. The bottom of the column is a single nozzle gas distributor through which gas is introduced into the column. The gas nozzle is connected to a flow meter which measures the gas flow rate. A pressure gauge connected to the flow meter reads the pressure of the gas. The liquid within the column was static (i.e., no liquid flow) prior to bubbling of gas through it. Hence, in this study, there was no variation in the liquid flow rate, but rather a variation of the gas flow rate. A twin plane Electrical Capacitance Tomography (ECT) sensor with an interplanar spacing of 30 mm was used. Electrical capacitance tomography is an advanced non-intrusive instrumentation technique which can be used for both imaging and velocity measurements in flows of mixtures of two non-conducting materials undertaken in real time and over an arbitrary number of zones in the flow cross section. The sensor used is an 8-electrode system which gives 28 measurements relayed to the computer where image reconstruction occurs (see Fig. 3). Details of the experimental arrangements are given in Kajero *et al.* (2012).

The Phantom high-speed camera was used to take the video of what is happening in the column. The pictures were taken at a sample rate of 1000 pps (pictures per sec) with an exposure time of 60 μs. The geometry specified gives the image width by image height as 512×512 pixel. The Phantom high-speed camera control software, version 606, was used to analyze the video obtained.

IV. RESULTS AND DISCUSSION

From the analysis done using the probability density function of the void fraction traces, images from the ECT and the high-speed camera, the corresponding flow patterns for all the viscosities considered are obtained.

A. Flow pattern and bubble behavior in 5 mPa s silicone oil

Table I gives a summary of the flow pattern in 5 mPa s silicone oil from the high-speed camera and PDF. At a gas superficial velocity of 0.02–0.041 m/s, small spherical bubbles were observed from the high-speed camera and PDF, 0.054–0.138 m/s bigger spherical cap bubbles, while from 0.155 to 0.361 m/s, developing slug flow was observed. The transition region was between 0.138 and 0.155 m/s. At 0.155 m/s, slug flow starts appearing which is referred to as developing slug flow which are short aerated slugs, as described by Nydal (1992). At this point of developing slug flow, the deformed Taylor bubble was observed which occupied almost the whole diameter of the column, as seen from the high-speed camera. From the PDF, two peak regions were seen: a long peak and a short peak which indicate the commencement of slug flow.

The flow pattern obtained from the high-speed video camera is shown in Fig. 4.

TABLE I. Flow pattern in 5 mPa s silicone oil.

Run	Gas superficial velocity (m/s)	Visual observation via high speed camera images	PDF
1–3	0.02–0.041	Small spherical cap bubble	Small spherical cap bubble
4–9	0.054–0.138	Bigger spherical cap bubble	Bigger spherical cap bubble
		Transition region	
10–15	0.155–0.361	Developing slug flow (deformed Taylor bubble)	Developing slug flow (deformed Taylor bubble)

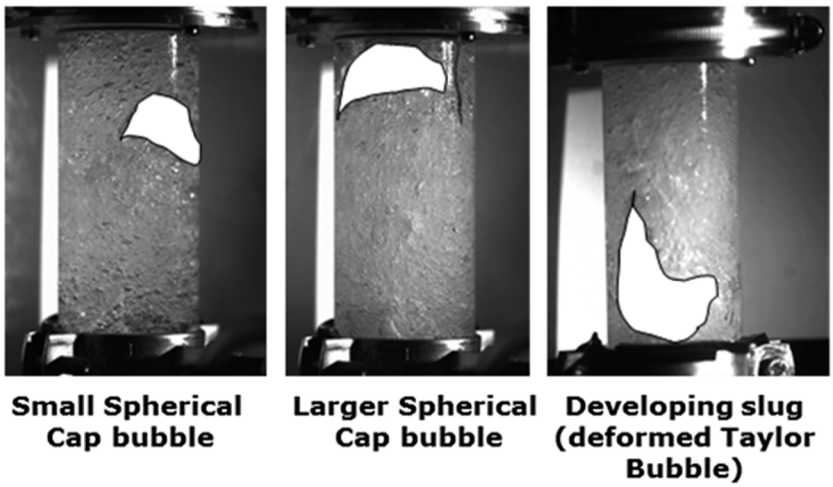

FIG. 4. Flow patterns from the high-speed camera images (5 mPa s).

The flow pattern in Table I is confirmed from the probability density function (PDF) plots shown in Fig. 5. This further accounts for the small and bigger spherical cap bubbles and the developing slugs (deformed Taylor bubbles) captured from the high-speed camera images. The PDF reveals that as gas superficial velocity increases, the PDF value on the y-axis

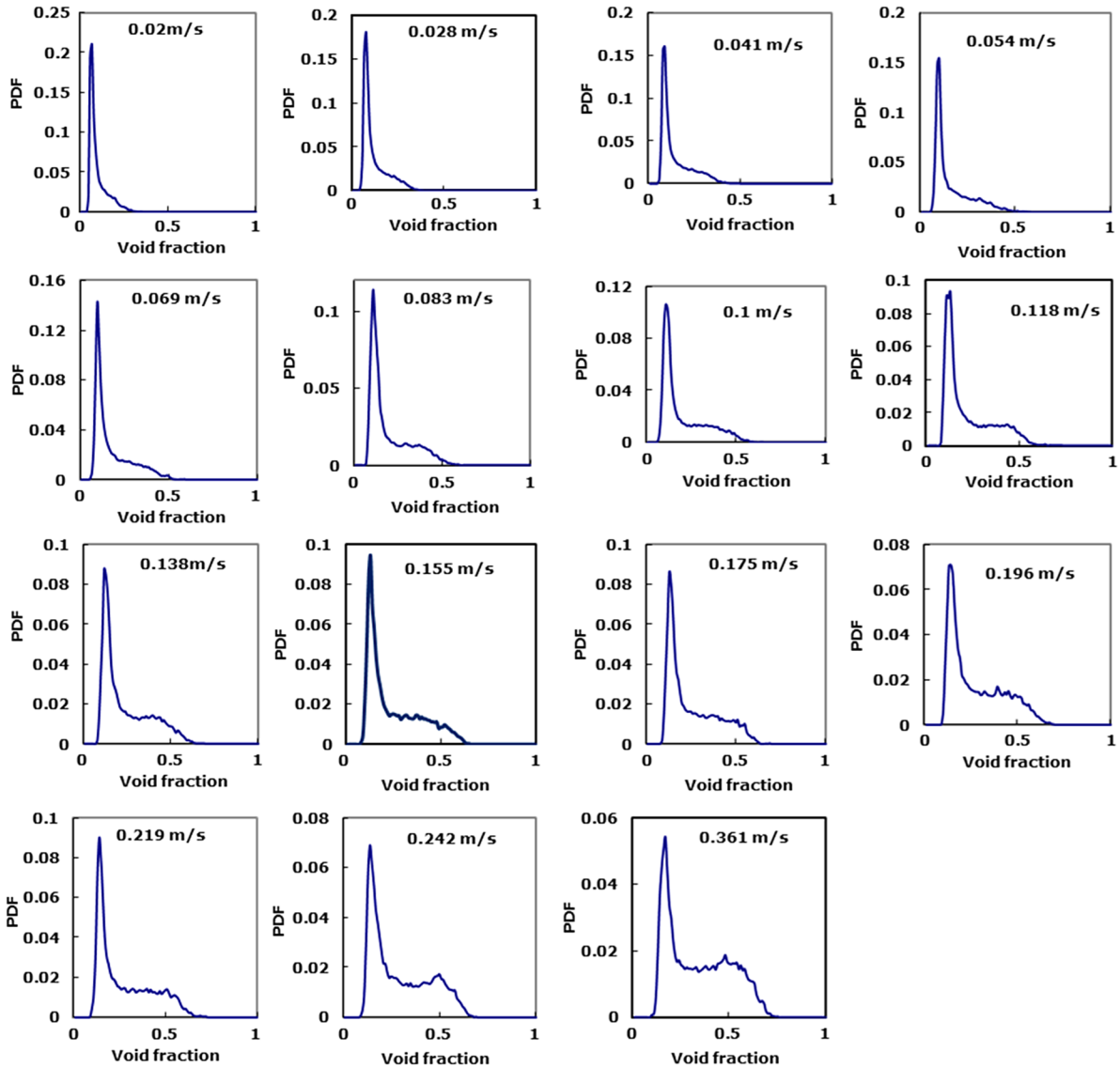

FIG. 5. Probability density function (PDF) plots for 5 mPa s at gas superficial velocities of 0.02–0.361 m/s.

TABLE II. Flow pattern in 100 mPa s silicone oil.

Run	Gas superficial velocity (m/s)	Visual observation via high speed camera images	PDF
1–3	0.02–0.041	Small spherical cap bubble	Small spherical cap bubble
4–9	0.054–0.138	Bigger spherical cap bubble	Bigger spherical cap bubble
		Transition region	
10–15	0.155–0.361	Developing slug flow (deformed Taylor bubbles)	Developing slug flow (deformed Taylor bubbles)

decreases which implies a decrease in the length of the long peak with low void fractions and an increase in the length of the short peak, with higher void fractions. Hence, the flow patterns start with a small spherical cap which subsequently becomes a bigger spherical cap, and then deformed Taylor bubbles. In essence, higher PDF trace values with a long peak of low void fractions account for a small spherical cap; lower PDF trace values with a reduced peak account for a bigger spherical cap, while a further reduction in the PDF trace values and its peak with an additional short peak upstream (with higher void fractions) accounts for deformed Taylor bubbles.

From the probability density function (PDF) plots, it can be seen that from gas superficial velocities of 0.02–0.041 m/s, the PDF is singled peaked with a small tail indicating small spherical cap bubbles. From 0.054 to 0.138 m/s, two peaks exist, a long peak and a short peak with the length of the short peak increasing with an increase in the gas superficial velocity. From 0.155 to 0.361 m/s, the length of the short peaks becomes more pronounced increasing as gas superficial velocity increases. Two major pieces of information can be inferred from the PDF, which are as follows:

1. The tail of the short peak extended on the void fraction axis increases with an increase in the gas superficial velocity. Hence, this indicates an increase in the void fraction in the Taylor bubble. The void fraction in the Taylor bubble is the fraction of gas in the Taylor bubble. It can also be expressed as the ratio of the area of gas in the Taylor bubble to the area of gas in the column containing gas and liquid.
2. The long peak from which the void fraction in liquid slugs is also obtained indicates a seemingly increase in void fraction in liquid slugs as gas superficial velocity increases.

B. Flow pattern and bubble behavior in 100 mPa s silicone oil

The pattern obtained in 100 mPa s silicone oil is similar to that of 5 mPa s as shown in Table II with the transition region occurring between gas superficial velocities of 0.138 and 0.155 m/s.

The flow patterns are shown by the high-speed camera images in Fig. 6.

These correlate with the probability density function (PDF) plots shown in Fig. 7.

A good study of the PDF obtained for 100 mPa s silicone oil looks similar to that of 5 mPa s. Hence, the same inference can be drawn from it.

C. Flow pattern and bubble behavior in 1000 mPa s silicone oil

Table III gives a summary of the flow pattern in 1000 mPa s silicone oil from visual observation via the high-speed camera images and PDF. From the PDF, the flow pattern is characterized by developing slug flow (Sven, 1999) from a gas superficial velocity of 0.02 m/s–0.028 m/s, and slug flow from a gas superficial velocity of 0.041–0.361 m/s. The developing slug flow from the PDF is characterized by a long peak and a short peak, while in the fully developed slug flow, the short peak becomes longer. By visual observation using the high-speed video camera, the developing slug flow is characterized by short Taylor bubbles, while the fully developed slug flow by long Taylor bubbles. This is indicated by the probability density function (PDF) plots shown in Fig. 8.

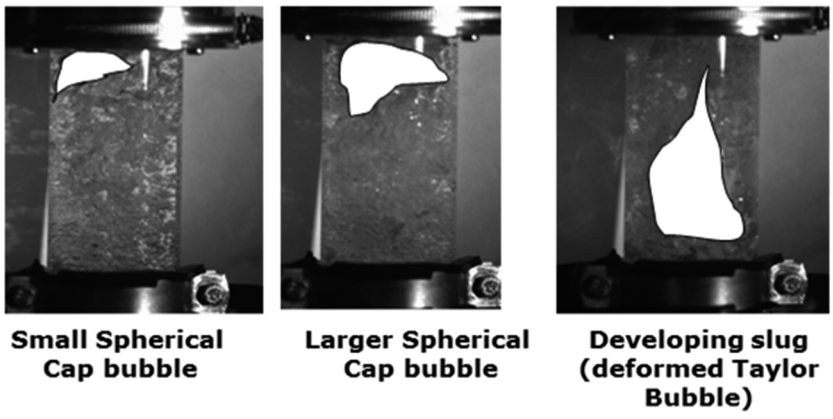

FIG. 6. Flow patterns from the high-speed camera images (100 mPa s).

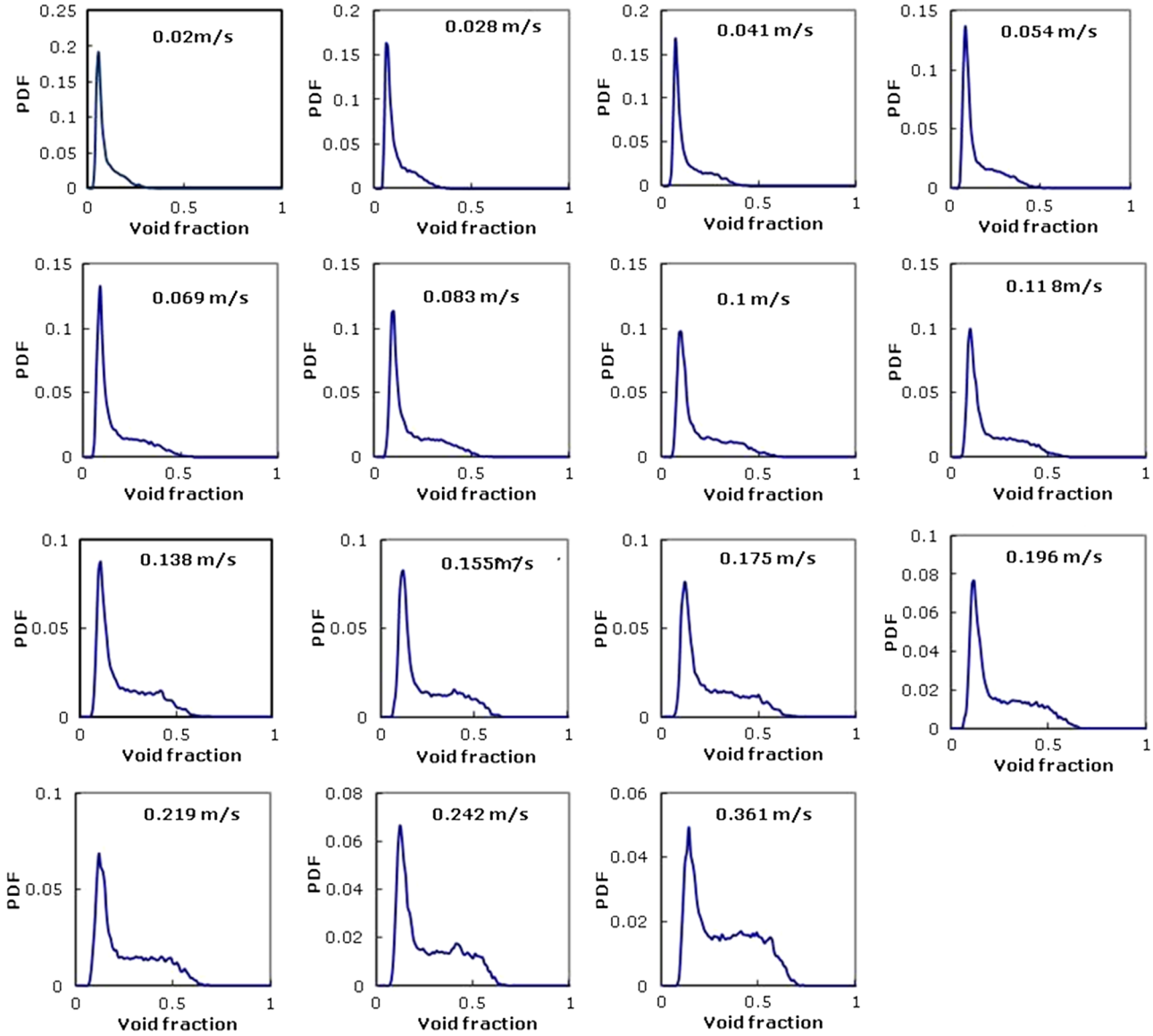

FIG. 7. Probability density function (PDF) plots for 100 mPa s at gas superficial velocities of 0.02–0.361 m/s.

From the PDF plots for 1000 mPa s, for 0.02 and 0.028 m/s gas superficial velocities, there exists a long peak (of liquid slugs) and short peak (of Taylor bubbles). Due to the observed short peak, the flow pattern is said to be developing slug. As the gas superficial velocity increases, this long peak reduces in magnitude, while the short peak increases which indicates the existence of developed slugs. The long peak of liquid slugs in Fig. 8 shows very small gas fraction (i.e., contain more of liquid); hence, the void fraction tends to zero. When the PDF is compared with the high-speed camera video images shown in Fig. 9, the decrease in the long peak and the increase in the short peak are accounted for by the decrease in the length of the liquid slug and the increase in the length of the Taylor bubble. At a point, 0.083 m/s gas superficial velocity to be precise, the length of the liquid slug becomes equal to the length of the Taylor bubble which leads to a decreasing short peak for liquid slugs and an increasing long peak for Taylor bubbles. This is also confirmed from the high-speed video camera images in Fig. 9. From the proposition of Costigan and Whalley (1997), this seems to be synonymous to the unstable slug which was not so obvious from the high-speed camera video images.

TABLE III. Flow pattern in 1000 mPa s silicone oil.

Run	Gas superficial velocity (m/s)	Visual observation via high speed camera images	PDF
1–2	0.02–0.028	Developing slug flow	Developing slug flow
3–15	0.041–0.361	Slug flow	Slug flow

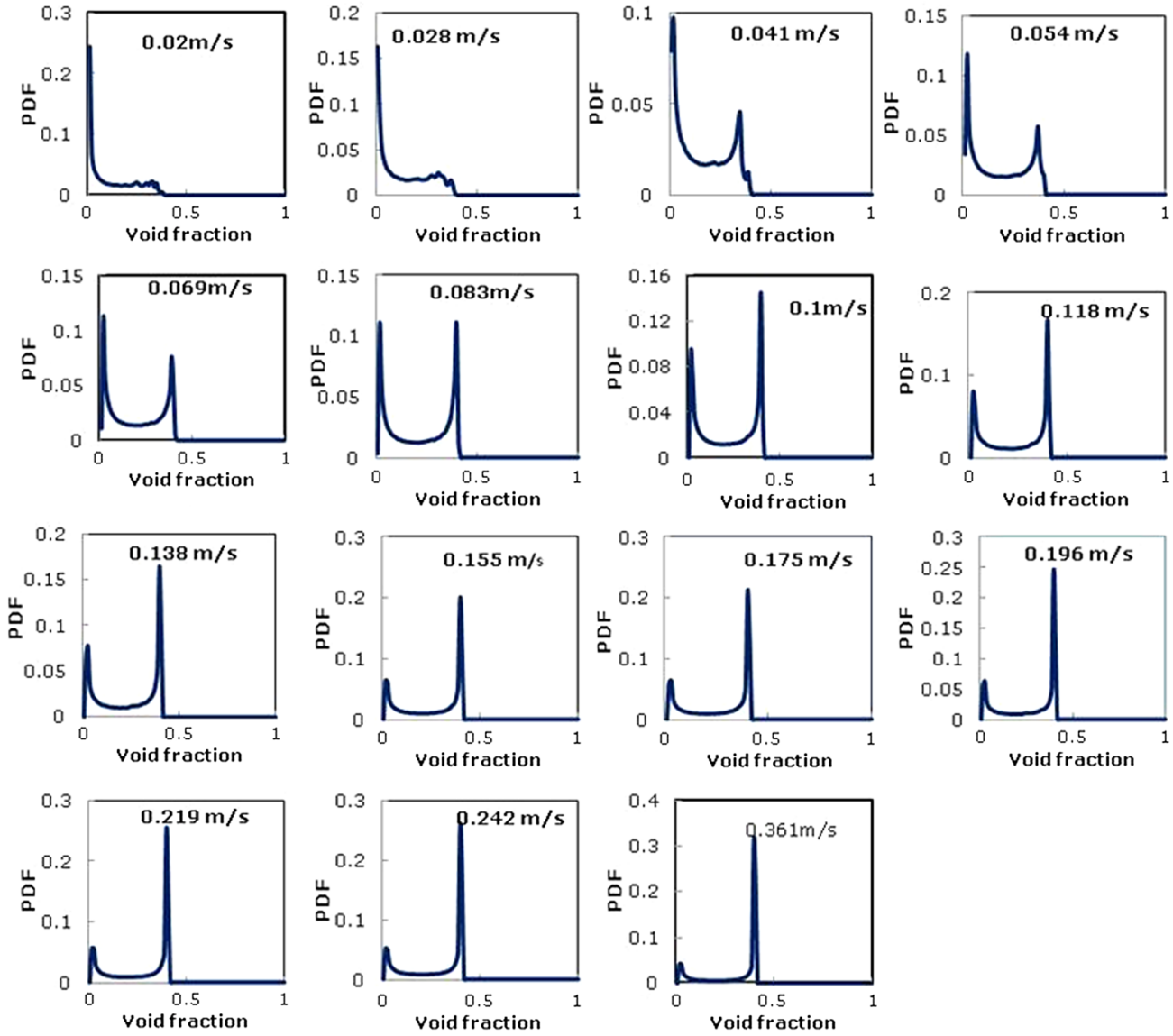

FIG. 8. Probability density function (PDF) plots for 1000 mPa s at superficial gas velocities of 0.02–0.361 m/s.

The void fraction in liquid slugs and Taylor bubbles seems to increase and eventually appears to stabilize, becoming almost constant as the gas superficial velocity increases. This indicates that a point is reached when increasing the supply of gas seems not to influence the void fraction in the liquid slug and Taylor bubble. Here, the critical void fraction in the liquid

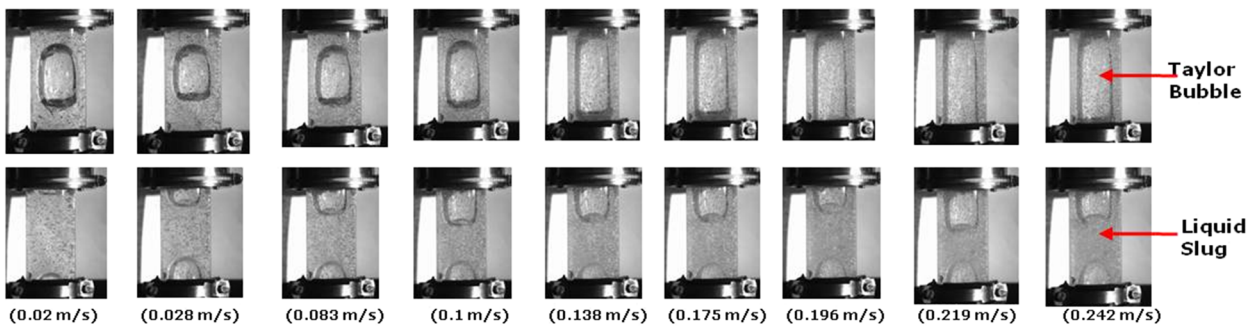

FIG. 9. Variation in the length of the Taylor bubble and liquid slug as the gas superficial velocity increases. At 0.083 m/s, the length of the Taylor bubble and liquid slug appears to be the same.

slug and Taylor bubble seems to be reached, and this could be due to a balance between the viscous force and surface tension force.

D. Flow pattern and bubble behavior in 5000 mPa s silicone oil

The flow patterns in 5000 mPa s silicone oil are similar to what was observed in that of 1000 mPa s from a gas superficial velocity of 0.1 m/s. A comparison of the PDFs with the high-speed camera images can lead to the classification of 0.02–0.028 m/s gas superficial velocities as developing slug flow, while 0.041–0.361 m/s are classified as slug flow, just like that of 1000 mPa s. The PDF of various viscosities at different gas superficial velocities of 0.02–0.361 m/s is shown in Fig. 10.

From the PDF for 5000 mPa s, at a gas superficial velocity of 0.02 m/s, the long peak of the Taylor bubble is a bit longer than that of the liquid slug. As the gas superficial velocity increases, the long peak of the Taylor bubble increases, while that of the liquid slug reduces which from high speed camera images implies increase in the length of the Taylor bubble and decrease in the length of the liquid slug (as shown by the high-speed camera images in Fig. 11) and a point is reached when there exists a small space between a leading and a trailing Taylor bubble, which implies an obvious decrease in the length of the liquid slug. The observed flow pattern in 5000 mPa s seems to be synonymous to what was described by Costigan and Whalley (1997) as the unstable slug though not so obvious from the high-speed camera. This deviation from the conventional [Costigan and Whalley (1997)] classification is probably due to the viscous nature of the liquid as compared with water. The air-water flow in Costigan and Whalley (1997) is inertia dominated (as the inverse dimensionless viscosity is greater than 300), while the air-silicone oil flow in 1000 and 5000 mPa s is viscous dominated.

The flow pattern categorization using the diameter ratio for each viscosity is given in Tables IV–VII.

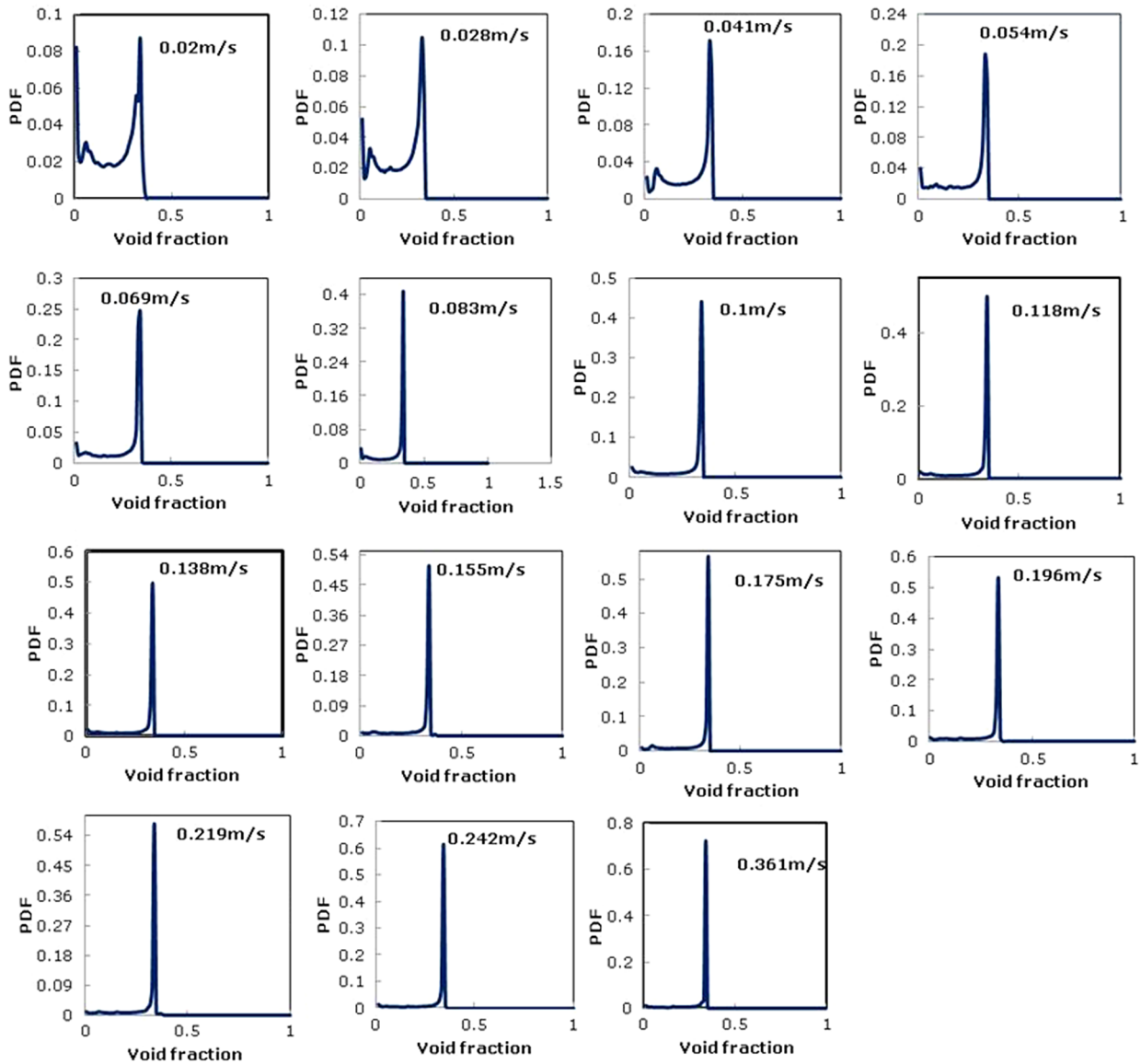

FIG. 10. Probability density function (PDF) plots for 5000 mPa s at gas superficial velocities of 0.02–0.361 m/s.

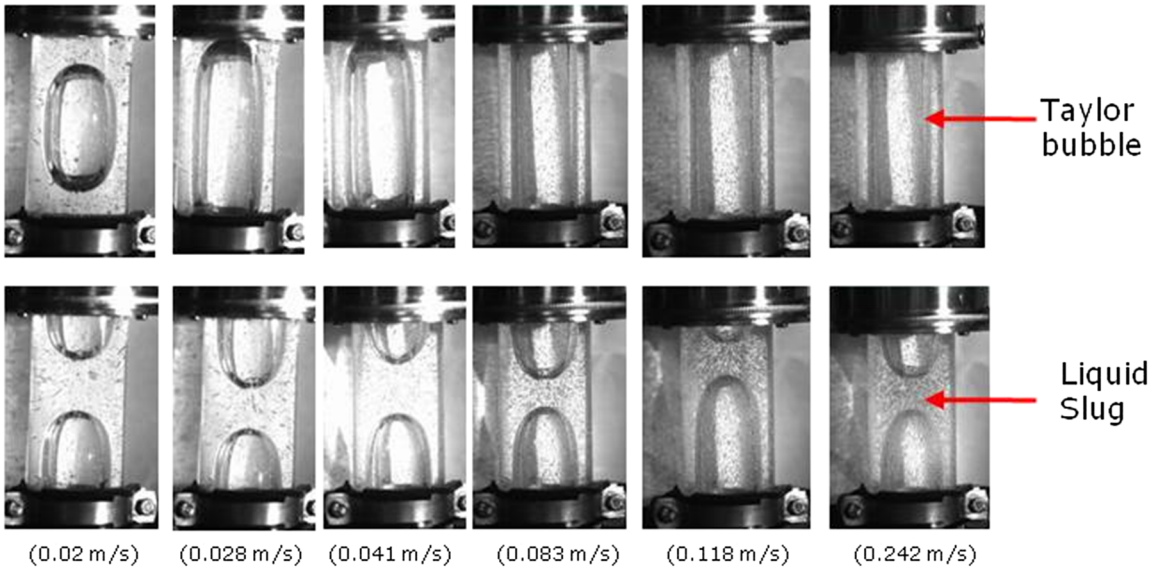

FIG. 11. Increasing length of the Taylor bubble and decreasing length of the liquid slug.

The study in this work reveals that the formation of large bubbles, i.e., Taylor bubbles become prominent with an increase in the liquid viscosity, with highly viscous liquids having more tendency for such. Hence, as the viscosity increases, the diameter of Taylor bubbles decreases. This is probably due to the domineering effect of viscous forces over surface tension forces. As the viscosity increases, it is expected that the cross-sectional area of the cylindrical portion of the Taylor bubble increases with an increase in the gas supply due to the increased gas production rate as the gas superficial velocity increases, hence causing more gas to occupy the cross-sectional area of the column. But the surface tension is not strong enough to enhance the expansion of the bubbles which could lead to an increase in the diameter and hence could not overcome the viscous forces arising from the viscous nature of the liquid.

TABLE IV. Flow pattern using the diameter ratio (5 mPa s).

Gas superficial velocity (m/s)	Diameter ratio range (m)	Flow pattern
0.02–0.118	0.45–0.59	Spherical cap bubble
0.138–0.361	0.64–0.71	Slug flow

TABLE V. Flow pattern using the diameter ratio (100 mPa s).

Gas superficial velocity (m/s)	Diameter ratio range (m)	Flow pattern
0.02–0.118	0.42–0.58	Spherical cap bubble
0.138–0.361	0.64–0.71	Slug flow

TABLE VI. Flow pattern using the diameter ratio (1000 mPa s).

Gas superficial velocity (m/s)	Diameter ratio range (m)	Flow pattern
0.02–0.361	0.6–0.63	Slug flow

TABLE VII. Flow pattern using diameter ratio (5000 mPa s).

Gas superficial velocity (m/s)	Diameter ratio range (m)	Flow pattern
0.02–0.361	0.6–0.61	Slug flow

E. Basis of categorization: Wall effect

According to Clift *et al.* (2005), when the diameter ratio exceeds a value of about 0.6, the tube or column diameter becomes the controlling length, governing the velocity and the frontal shape of a bubble or drops. At this point, the bubbles or drops are called slugs or Taylor bubbles which are usually bullet-shaped. A factor responsible for this categorization is the Wall effect. It arises from the proximity relationship between the column wall and diameter, which could influence the flow behavior and its associated characteristics or phenomenon such as coalescence, bubble size, bubble velocity, etc., within the column, most especially in a viscous medium (Ataíde *et al.*, 1999).

The wall effect is more pronounced in a small diameter column. As the column diameter decreases, the wall effect increases (Ruzicka *et al.*, 2001). Wall effects tend to affect the bubble rise velocity, when the ratio of the bubble diameter to column diameter is greater than 0.125 (Krishna *et al.*, 2001 and Heindel *et al.*, 2006), which implies the bubble should occupy a diameter of > 12.5% of the column diameter. The hindering of the bubble rise velocity increases as the viscosity increases, leading to an increase in the coalescence rate and hence the bubble size. This increase in the bubble size implies the formation of larger bubbles (Taylor bubbles) with an increase in the viscosity. This flow pattern categorization using the diameter ratio confirms the work of Hosoda *et al.* (2011).

The image display in single axial slice mode from the Plot3D program for ECT data showing an increase in the bubble size as the viscosity increases for a gas superficial velocity of 0.361 m/s is shown in Fig. 12. It likewise shows the

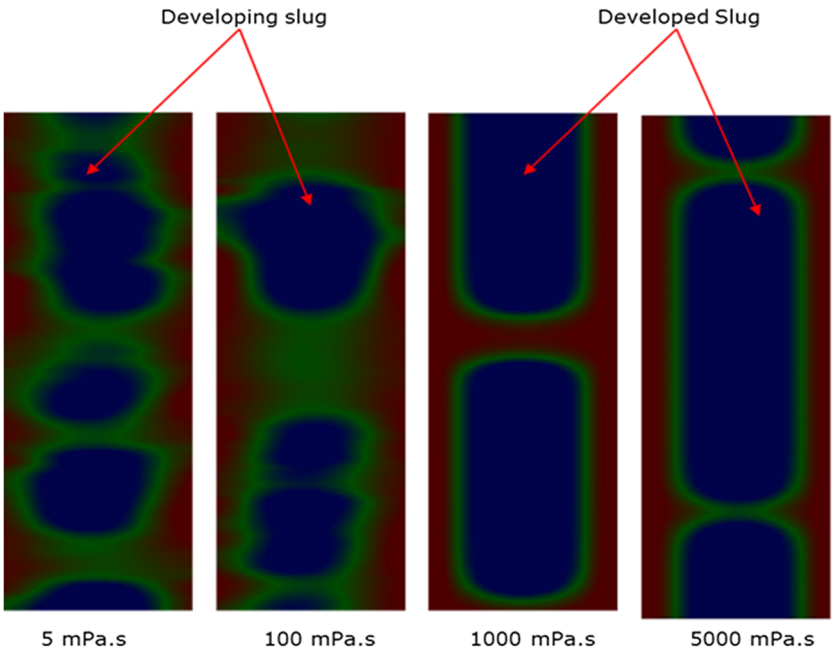

FIG. 12. Image display in single axial slice mode from the Plot3D program for ECT data showing an increase in the bubble size as the viscosity increases for a gas superficial velocity of 0.361 m/s.

transition from developing slugs to slugs. Figure 12 is a real-time ECT image of the cross-sectionally averaged void fraction spatial distribution. It provides both spatial distribution and time distribution of the void fraction.

The current work has been compared with that of Costigan and Whalley (1997) in terms of void fraction in liquid slugs and Taylor, as shown in Table VIII.

From Table VIII, it can be observed that the void fraction in liquid slugs and Taylor bubbles in the current study is lower than that of Costigan and Whalley (1997). This is probably due to the following reasons:

1. The use of high viscous liquids (5, 100, 1000, 5000 mPa s) compared with water (0.89 mPa s) used by Costigan and Whalley (1997). In Kajero *et al.* (2012), this was explained to be due to the domineering effect of viscous force over surface tension force. As the surface tension force is suppressed while the viscous force dominates, the rate of accumulation of voids decreases due to a decrease in the rate of coalescence and the rate of bubble entrainment into the liquid slug decreases. This phenomenon becomes more pronounced as the viscosity increases. Hence, 5 and 100 mPa s have higher void fraction in the liquid slugs and Taylor bubbles than 1000 and 5000 mPa s.
2. A lower range of gas superficial velocities were used in the current study (0.02–0.361 m/s) when compared with that of Costigan and Whalley (1997): 1–3.5 m/s. This is because the void fraction increases with an increase in the gas superficial velocity.

The void fraction in Taylor bubbles for a gas superficial velocity of 0.361 m/s (5 mPa s silicone oil) is about 0.5. This when compared with an estimated data from Abdulkadir (2011) appears to be relatively the same.

The change in the trend of the PDF, hence the flow pattern relative to the void fraction and gas superficial velocity, is shown in Fig. 13, considering a gas superficial velocity of 0.242 m/s. From Fig. 13, as the viscosity increases, the void fraction in the liquid slug and Taylor bubble seems to decrease.

TABLE VIII. Comparison of the classification of flow patterns from the current study with Costigan and Whalley (1997).

	Costigan and Whalley (1997)	Current study
Liquids and their viscosities	Water: 0.89 mPa s	Silicone oil: 5, 100, 1000 and 5000 mPa s
Flow patterns and associated void fractions	Spherical cap bubble • Liquid slugs ≥ 0.4 • Taylor bubble: 0.8 Stable slugs • Liquid slugs: 0.4 • Taylor bubble ≥ 0.8 Unstable slugs • Liquid slugs ≥ 0.4 • Taylor bubble < 0.8	Spherical cap bubble • Liquid slugs: 0.05–0.15 • Taylor bubble: 0.18–0.40 Developing slugs • Liquid slugs: 0.1–0.16 • Taylor bubble: 0.41–0.51 Slugs • Liquid slugs: 0.004–0.15 • Taylor bubble: 0.31–0.4

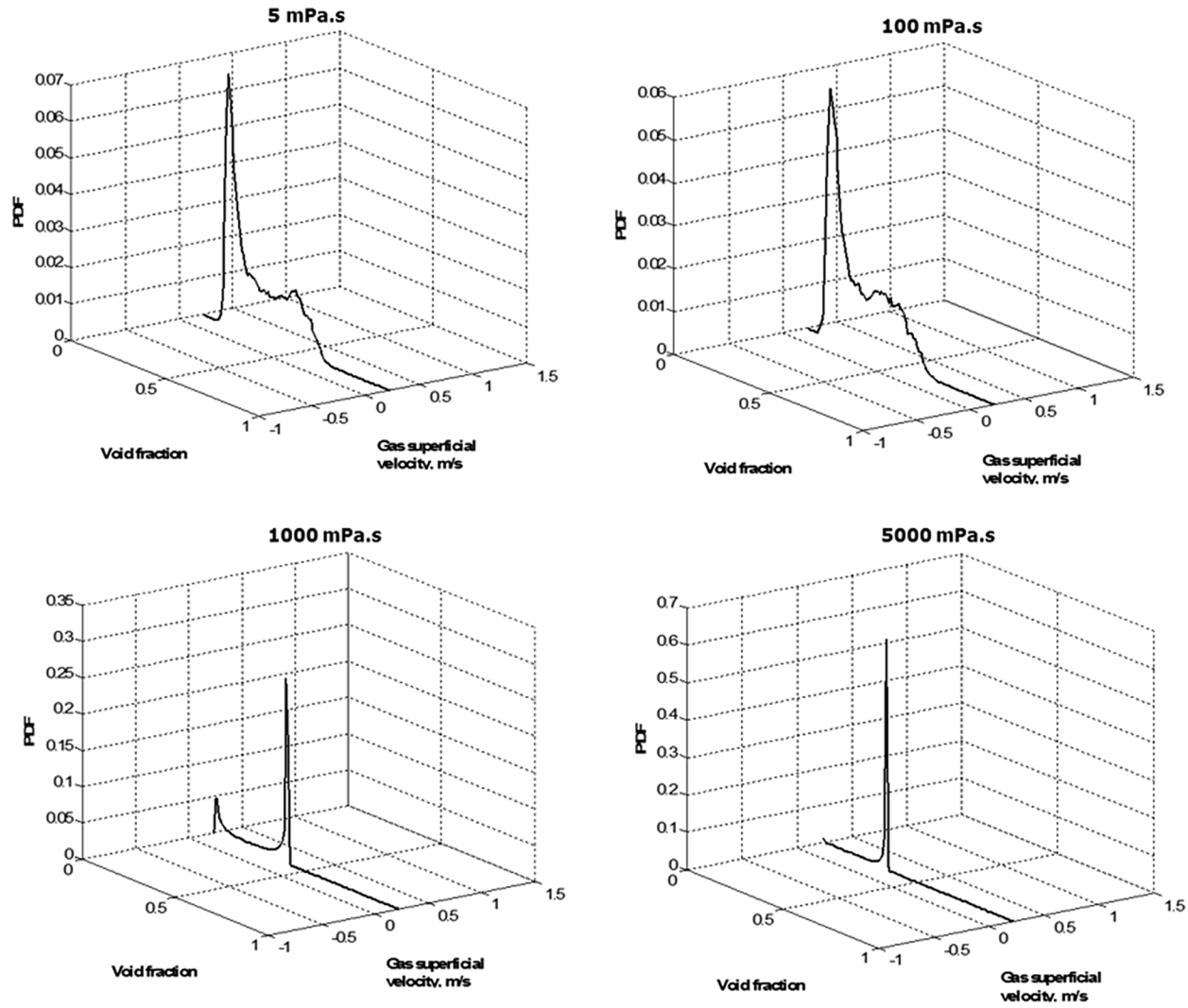

FIG. 13. Three-dimensional plot indicating variation in the flow pattern with an increase in the viscosity at a gas superficial velocity of 0.242 m/s.

The decrease in the void fraction in the liquid slug is due to the merging of the entrained big bubbles in the liquid slug with the succeeding Taylor bubbles leading to an increase in the length of Taylor bubbles and a decrease in the length and void fraction in the liquid slug. The decrease in the void fraction in Taylor bubbles was said to be due to the domineering effect of viscous force over the surface tension force according to Kajero *et al.* (2012).

The PDF, high-speed camera pictures, and 3D-plot from ECT have been compared to elaborate on the observed flow patterns at different viscosities as shown in Fig. 14.

F. Bubble shape and characteristics

The shape of the Taylor bubble has been categorized by Fabre and Line (1992) depending on whether or not viscous force is negligible, based on the shape of the rear end of the bubble. They categorized them into a prolate spheroid and an oblate spheroid. These were obtained from the high-speed video camera in this current work, as shown in Fig. 15.

Prolate spheroid occurs when viscous force is negligible wherein the bubble has a flat back or a flat trailing edge. This also confirms Wallis (1969). Fabre and Line (1992) claimed the occurrence of flow separation at this region. In the current experiment carried out, the flat trailing edge was observed in 1000 mPa s from the High-Speed video camera images and it is expected that viscous force is dominant contrary to the proposition of Fabre and Line (1992).

Oblate spheroid occurs when viscous force is significant, and the bubble back is curved or spherical (rounded at both ends) following a standing wavelet on the film (Goldsmith and Mason, 1962). The bubble has a convex interface when viewed from inside at its back (Clift *et al.*, 2005). The bubble rounded at both ends in this case also confirms the work of Wallis (1969).

The observed images for both prolate spheroid and oblate spheroid further confirm the work of Bugg *et al.* (1998).

Fabre and Line (1992) proposed that a two-phase slug flow is viscous force negligible (inertia controlling regime) when the inverse dimensionless viscosity, N_f, and Eotovos number, Eo, are both greater than 300, while it is viscous force dominant (viscous controlling regime) when the inverse dimensionless viscosity, N_f, is less than 2. Wallis (1969) proposed that at low values of N_f (<300) or for values of the Reynolds

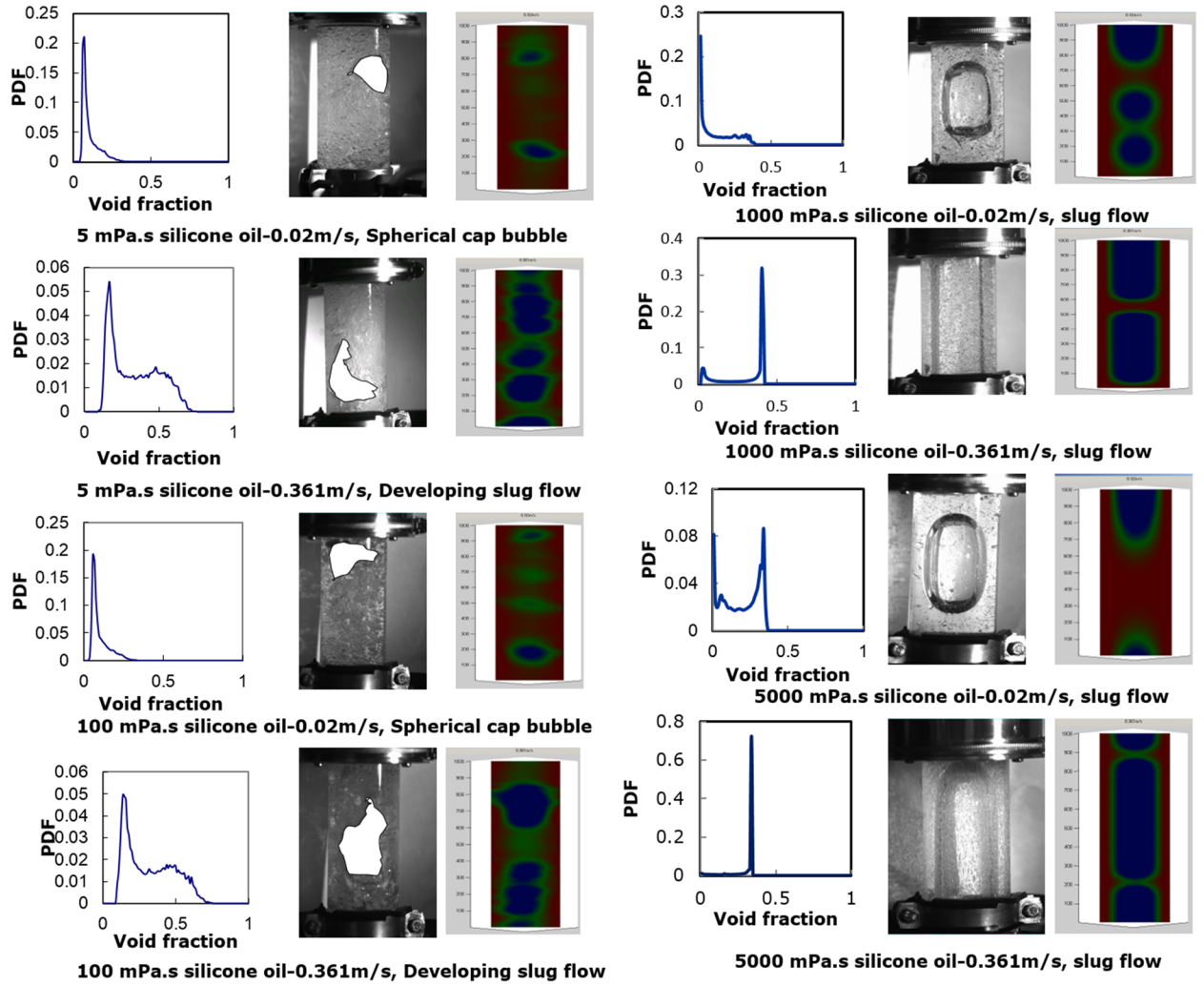

FIG. 14. Flow patterns in 5, 100, 1000, and 5000 mPa s silicone oil, as observed from the PDF, high speed camera pictures, and 3D-plot from ECT, respectively.

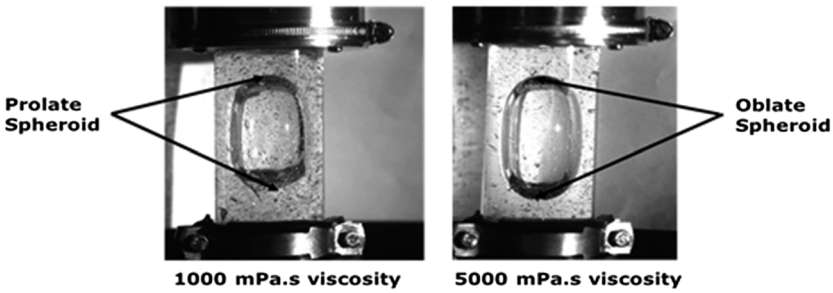

FIG. 15. Prolate spheroid and oblate spheroid in 1000 and 5000 mPa s viscosities, respectively.

number less than 8000, viscous force prevails. Using the inverse dimensionless viscosity and Eotovos number in the current work, the bubbles obtained can be characterized, as shown in Table IX.

The 5 and 100 mPa s are characterized by small and large spherical bubbles and developing slugs as the gas superficial velocity increases, while 1000 and 5000 mPa s are characterized by short and long Taylor bubbles as the gas superficial velocity increases. The developing slug in 5 and 100 mPa s appears to be in the form of deformed Taylor bubbles. This is because the slug flow is yet to be fully developed.

G. Coalescence

The formation of spherical cap bubbles and Taylor bubbles is based on the process of coalescence. A typical observation of coalescence from the high-speed video camera in gas-liquid flow in 1000 mPa s silicone oil is shown in Fig. 16.

From Fig. 16, the observed process of coalescence can be explained as follows:

(a) The "leading" and "trailing" bubbles gradually approach each other to coalesce.

TABLE IX. Bubble characteristics in terms of inverse dimensionless viscosity and Eotovos number.

Viscosity (mPa s)	Is $N_f > 300$ and $E_o > 100$? (viscous force negligible)	Is $N_f < 300$ and $E_o < 100$? (viscous force dominant)	Outcome
5	Yes: $N_f = 6408$, Eo = 1139	No	Viscous force negligible (inertia controlled regime)
100	Yes: $N_f = 3379$, Eo = 1132	No	Viscous force negligible (inertia controlled regime)
1000	Satisfies $E_o > 100$: $E_o = 1122$ Does not satisfy $N_f > 300$: $N_f = 34$	$N_f < 300$	Viscous force is dominant
5000	Satisfies $E_o > 100$: $E_o = 1111$ Does not satisfy $N_f > 300$: $N_f = 7$	$N_f < 300$	Viscous force is dominant

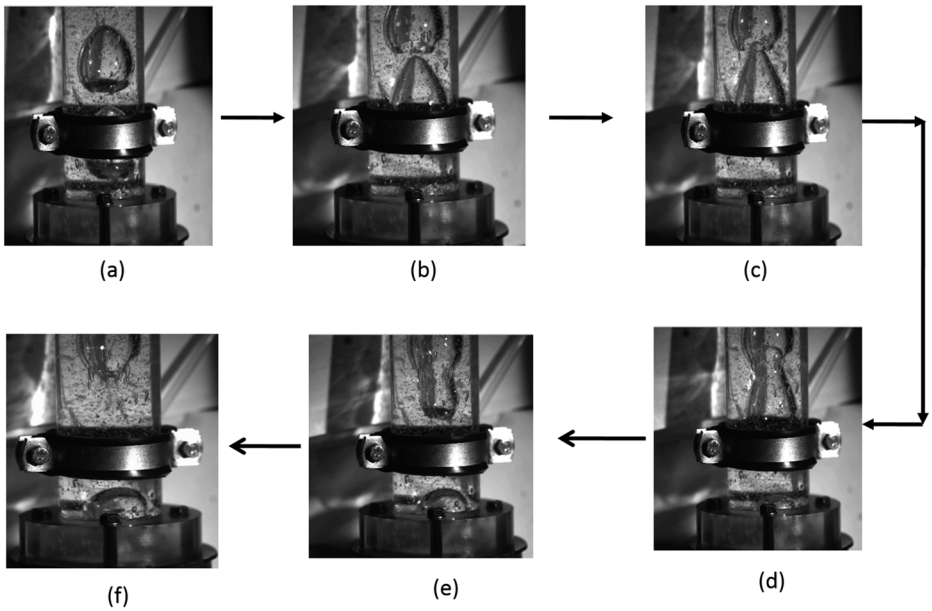

FIG. 16. Coalescence in 1000 mPa s.

(b) and (c) The "trailing" bubble extends at the head region to join with the leading bubble.
(d) The leading and trailing bubble collides trapping a small amount of liquid between them.
(e) The leading and trailing bubble merges further.
(f) The larger bubble is formed due to coalescence.

At very low gas superficial velocity (probably less than 0.02 m/s, the minimum used in this work), for the low viscous flow, it is anticipated that there will be bubbles with different rise velocities and hence increased rate of bubble collision when compared with bubbles that are uniformly sized. This growth of bubbles via collision continues until some large bubbles begin to take the form of a cap. The small bubbles in the wake of the cap bubble travel until they merge with the cap. The growth of the cap bubbles continues as the gas superficial velocity increases leading to the formation of Taylor bubbles which could be deformed (as in the case of 5 and 100 mPa s) or the normal Taylor bubble structure (as in the case of 1000 and 5000 mPa s).

H. Void fraction traces and their probability density functions

The PDF and time series plot have been placed side by side in Figs. 17 and 18 to give a vivid illustration of the change in the flow pattern and the mean void fraction at various viscosities with the gas superficial velocity as an increasing parameter.

Figures 17 and 18 show that as the gas superficial velocity and viscosity increase, the void fraction increases.

Further demonstration of growth from small spherical bubbles to bigger ones in 5 and 100 mPa s is shown in Figs. 19 and 20. It is observed that as the gas superficial velocity increases for each viscosity, the void fraction increases with a small spherical cap having low void fraction, while the bigger ones have higher void fraction. This increase in void fraction further accounts for the variation in spherical cap bubbles from smaller to bigger ones and from deformed Taylor bubbles to fully developed ones. Figures 17 and 18 also show the increase in the size of void fraction waves with an increase in the viscosity, which evidently affirms the increase in large bubble formation as the viscosity increases. This increase in void fraction can be accounted for via the wall effect, drag force, and surface tension effect.

1. Wall effect

As discussed in Sec. IV E, the wall effect has a significant influence on gas-liquid flow in a small diameter column, like the case of the current study with a column diameter of 50 mm. The wall effect promotes the bubble size increase, with the

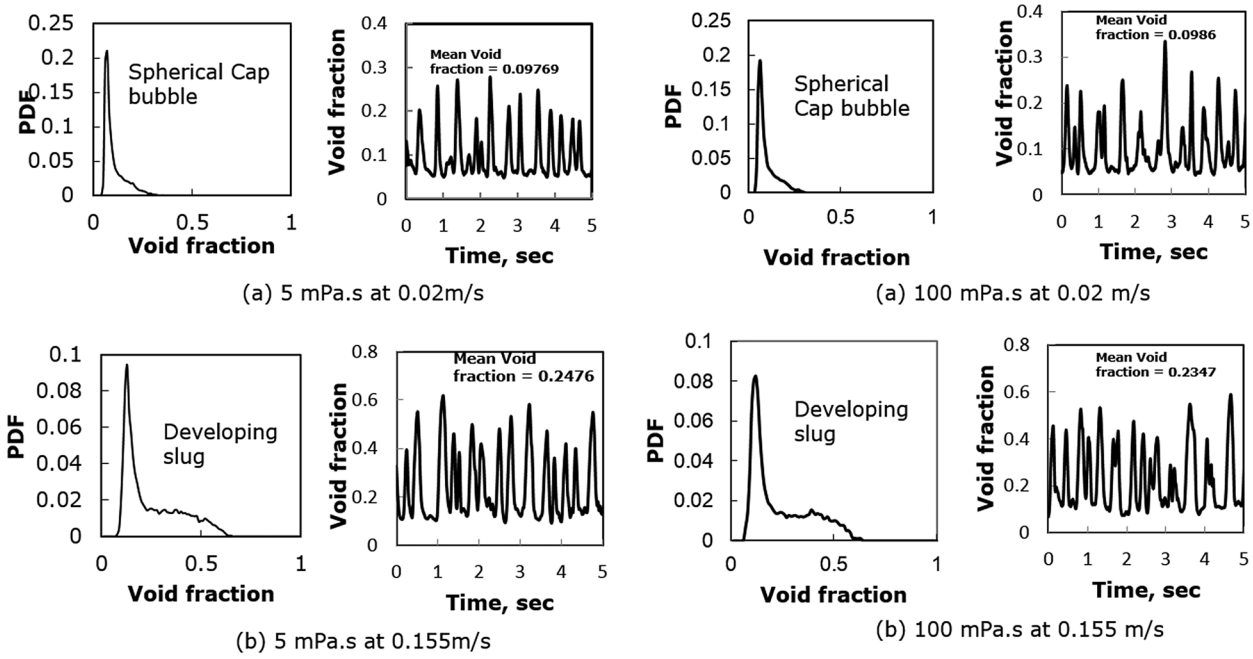

FIG. 17. PDF and void fraction traces of 5 and 100 mPa s at superficial gas velocities of (a) 0.02 and (b) 0.155 m/s, respectively.

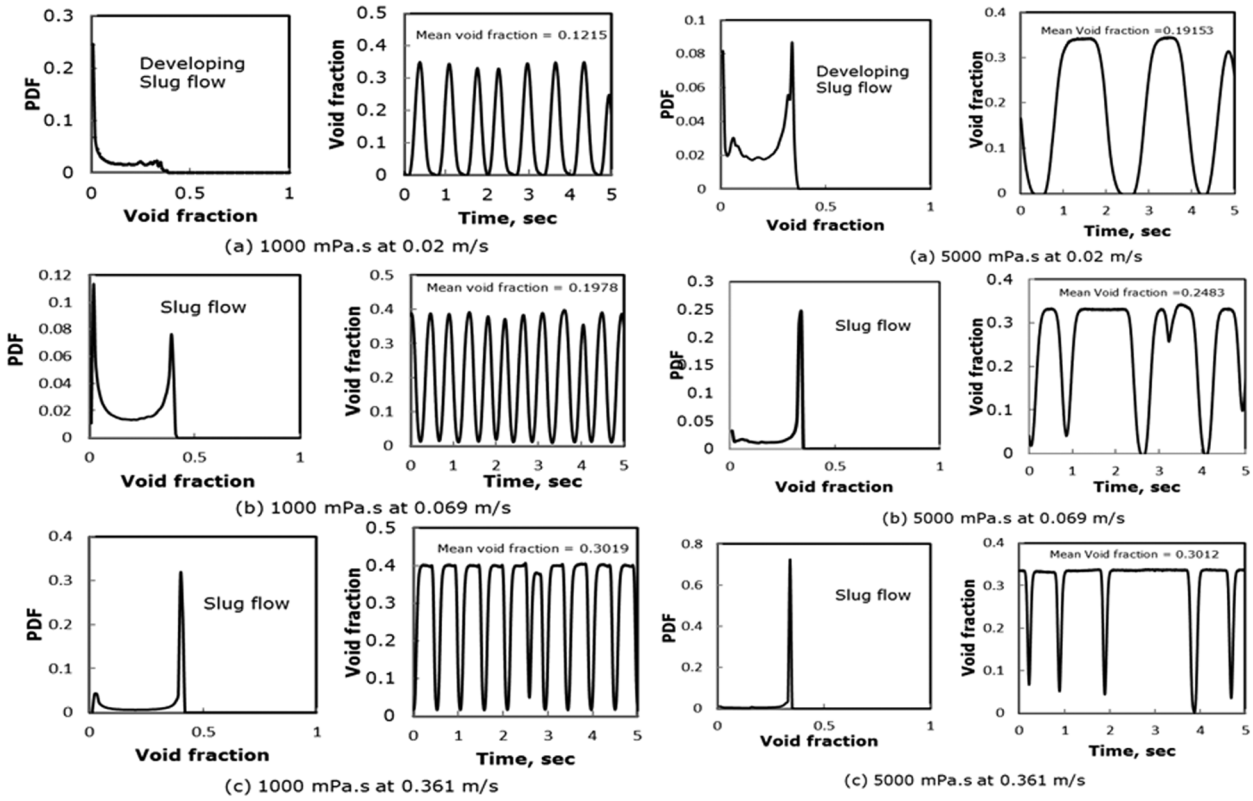

FIG. 18. PDF and void fraction traces of 1000 and 5000 mPa s at superficial gas velocities of (a) 0.02, (b) 0.069, and (c) 0.361 m/s, respectively.

formation of larger bubbles as the viscosity increases, and hence an increase in void fraction.

2. Effect of drag force

Drag force is the force which opposes the motion of the bubble through the liquid. From the Stokes law, drag force is directly proportional to liquid viscosity; hence, as the viscosity increases, the drag force increases due to the increase in the resistance offered by the liquid. As the drag forces increases, the rate at which the bubble rises through the liquid decreases which thereby leads to a decrease in the rise velocity of the bubbles. This eventually leads to an increase in bubble

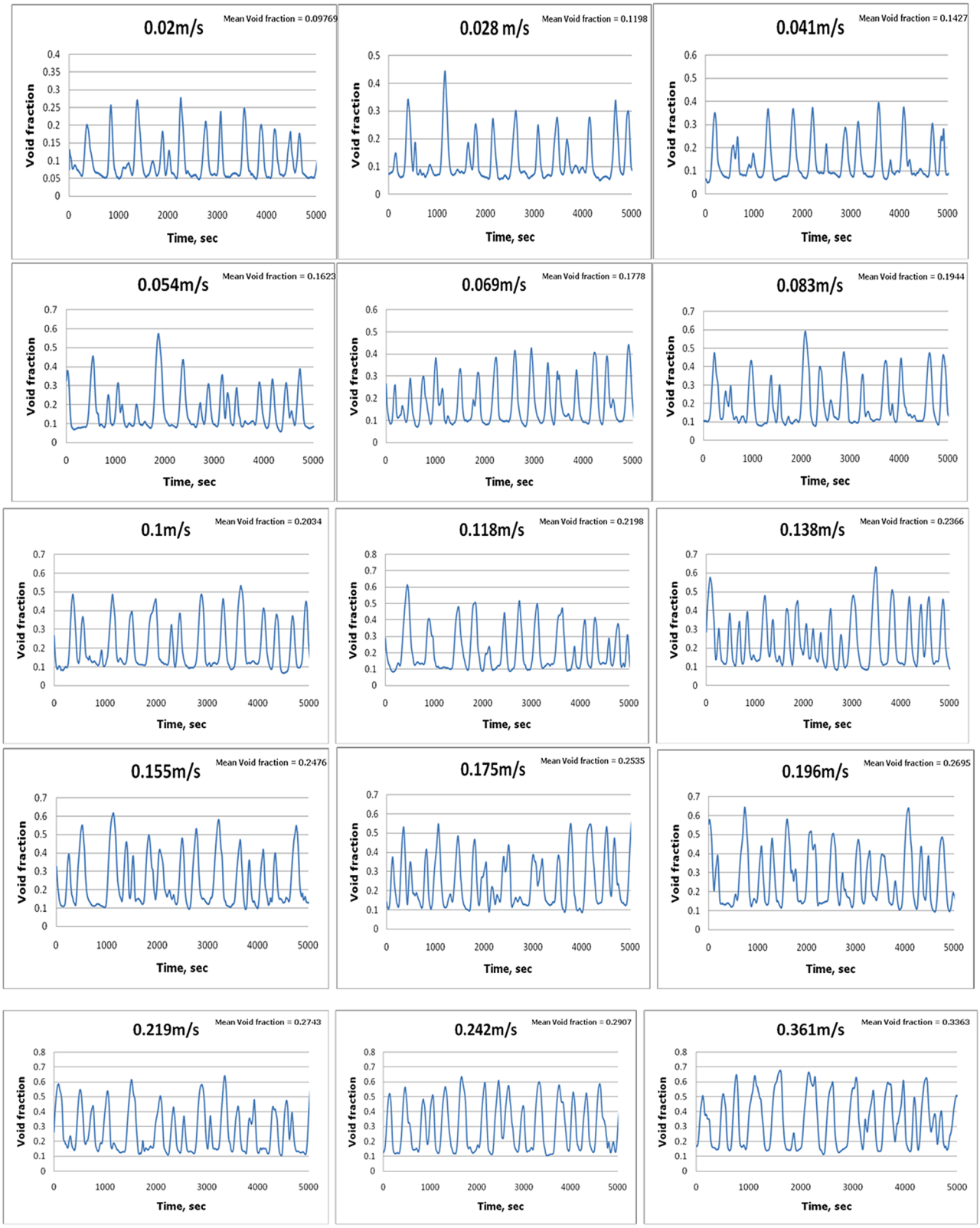

FIG. 19. Variation in void fraction with gas superficial velocity for 5 mPa s.

coalescence, which in large diameter pipe or column leads to a decrease in void fraction, whereas in the small diameter column, the increase in coalescence leads to an increase in the bubble size causing the bubble to occupy almost the whole cross section of the column, hence an increase in void fraction. See Sec. IV G for a discussion on bubble coalescence (Omeberi-Iyari and Azzopardi, 2007; Ruzicka *et al.*, 2003; Taitel *et al.*, 1980; and White and Beardmore, 1962).

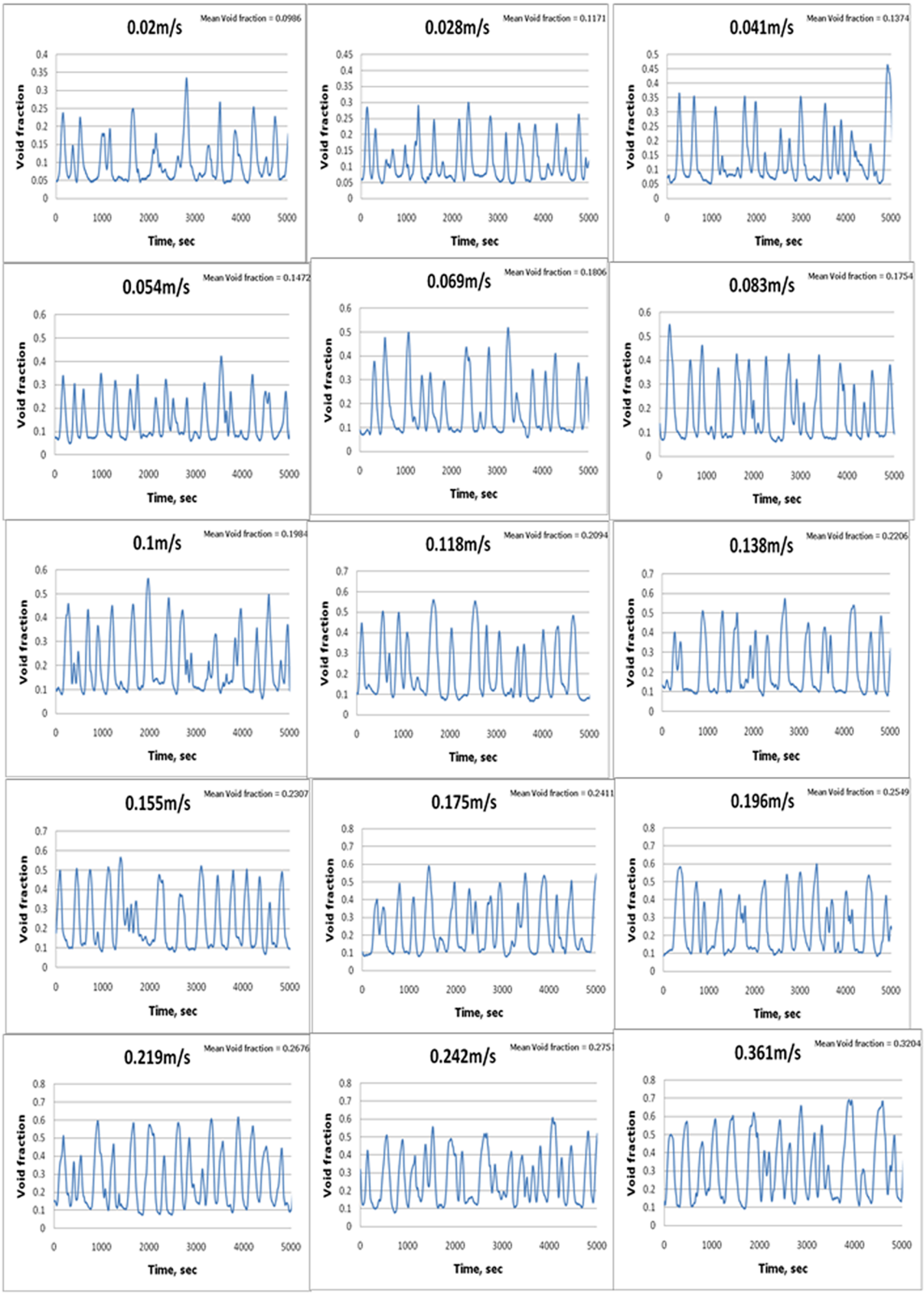

FIG. 20. Variation in void fraction with gas superficial velocity for 100 mPa s.

3. *Effect of surface tension force*

The increase in void fraction with an increase in viscosity can also be explained based on the effect of surface tension force. Surface tension force causes the fluid to pull together into spherical forms (spherical cap) or Taylor bubbles. As the viscosity of silicone oil increases from 5 to 5000 mPa s, the surface tension force increases. This contributes to the increase in the bubble size via an increase in the degree of cohesion of the bubbles and hence an increase in the

extent to which the agglomerate of bubbles (which occurs because of coalescence) is held together as cap bubbles or Taylor bubbles. This eventually leads to an increase in void fraction.

V. CONCLUSION

The conclusions drawn from this study are as follows:

1. From the high-speed video camera images, probability density function (PDF), void fraction traces, ECT image display, and Clift *et al.* (2005) diameter ratio,
   a. the flow patterns in 5 and 100 mPa s varied from small spherical cap bubbles to large spherical cap bubbles and then developing slug flow (deformed or short aerated slugs) as the gas superficial velocity increases;
   b. the slug flow patterns in 1000 and 5000 mPa s varied from developing slug to slug flow as the gas superficial velocity increases;
   c. as the viscosity increases, the appearance of spherical cap bubbles decreases, while the slug flow tendency increases; hence, slug flow tendency is directly proportional to the liquid viscosity;
   d. the variation from small spherical cap bubbles to bigger ones, deformed Taylor bubbles, and developed Taylor bubbles is due to the increase in void fraction with an increase in the liquid viscosity; this was accounted for by the wall effect, the drag force, and the surface tension force;
2. Liquid viscosities of 5 and 100 mPa s were observed to be viscous force negligible (inertia-controlled regime), while 1000 and 5000 mPa s were observed to be viscous force dominant (viscous controlled regime).
3. Void fraction in liquid slugs and Taylor bubbles is lower in the viscous liquids (5, 100, 1000, and 5000 mPa s) considered within a low range of gas superficial velocities, as compared with low viscous liquid like water within a high gas superficial velocity [as in the case of Costigan and Whalley (1997)].
4. Prolate spheroid shaped Taylor bubbles were observed in 1000 mPa s with a flat trailing edge or back, while oblate spheroid shaped Taylor bubbles were observed in 5000 mPa s with a curved or spherical back. This was obvious from the high-speed camera video. It can hence be inferred that the appearance of oblate spheroid Taylor bubbles is more pronounced in highly viscous liquids.

ACKNOWLEDGMENTS

This publication is in loving memory of the late Professor Barry Azzopardi.

Abdulkadir, M., "Experimental and computational fluid dynamics (CFD) studies of gas-liquid flow in bends," Ph.D. thesis, University of Nottingham, 2011.

Apazidis, N., "Numerical investigation of shock induced bubble collapse in water," Phys. Fluids **28**, 046101 (2016).

Ataíde, C. H., Pereira, F. A. R., and Barrozo, M. A. S., "Wall effects on the terminal velocity of spherical particles in Newtonian and non-Newtonian fluids," Braz. J. Chem. Eng. **16**(4), 387–394 (1999).

Azzopardi, B. J., Pioli, L. A., and Abdulkareem, L. A., "The properties of large bubbles rising in very viscous liquids in vertical columns," Int. J. Multiphase Flow **67**, 160–173 (2014).

Bousman, W. S., McQuillan, J. B., and White, L. C., "Gas-liquid flow patterns in microgravity: Effects of tube diameter, liquid viscosity and surface tension," Int. J. Multiphase Flow **22**(6), 1035–1053 (1996).

Bugg, J. D., Mack, K., and Rezkallah, K. S., "A numerical model of Taylor bubbles rising through stagnant liquids in vertical tubes," Int. J. Multiphase Flow **24**(2), 271–281 (1998).

Clift, R., Grace, J. R., Weber, M. E., and Weber, M. F., *Bubbles, Drops and Particles* (Dover Publications, Inc., New York, 2005).

Costigan, G. and Whalley, P. B., "Slug flow regime identification from dynamic void fraction measurements in vertical air-water flows," Int. J. Multiphase Flow **23**(2), 263–282 (1997).

Cui, P., Wang, Q. X., Wang, S. P., and Zhang, A. M., "Experimental study on interaction and coalescence of synchronized multiple bubbles," Phys. Fluids **28**, 012103 (2016).

Dabiri, S. and Bhuvankar, P., "Scaling law for bubbles rising near vertical walls," Phys. Fluids **28**, 062101 (2016).

Fabre, J. and Line, A., "Modelling of two-phase slug flow," Annu. Rev. Fluid Mech. **24**, 21–46 (1992).

Furukawa, T., "Effect of liquid viscosity on liquid-lump velocity in vertical upward gas-liquid two-phase flow, velocity characteristics of the long-life liquid lump," Jpn. J. Multiphase Flow **9**, 121–131 (1995).

Furukawa, T. and Fukan, T., "Effects of liquid viscosity on flow patterns in vertical upward gas-liquid two-phase flow," Int. J. Multiphase Flow **27**, 1109–1126 (2001).

Goldsmith, H. L. and Mason, S. G., "The movement of single large bubbles in closed vertical tubes," J. Fluid Mech. **14**, 42–58 (1962).

Heindel, T. J., Xuefeng, S., Hol, P. D., Talcott, S. M., and Staudt, A. K., "The effect of bubble column diameter on gas holdup in fiber suspensions," Chem. Eng. Sci. **61**, 3098–3104 (2006).

Hiroaki, M. and Kiyoshi, N., "Effect of liquid viscosity on flow patterns of gas-liquid two phase in a horizontal pipe," Int. J. Multiphase Flow **37**, 1277–1281 (2011).

Hosoda, S., Sakata, R., Hayashi, K., and Tomiyama, A., "Mass transfer from a bubble in a vertical pipe," in *ASME/JSME 2011 8th Thermal Engineering Joint Conference* (ASME, 2011), pp. T10183–T10189.

Jones, O. C. and Zuber, N., "The interrelation between void fraction fluctuations and flow patterns in two-phase flow," Int. J. Multiphase Flow **2**, 273–306 (1975).

Kajero, O. T., Abdulkareem, L., and Azzopardi, B. J., "Effect of liquid viscosity on slug flow in a small diameter bubble column," in Proceedings of the International Conference, Experimental Fluid Mechanics 2011, Jicin, Czech Republic, 2012.

Keska, J. K., Hincapie, J., and Jones, R., "Flow pattern changes influenced by variation of viscosities of a heterogeneous gas-liquid mixture flow in a vertical channel," Exp. Therm. Fluid Sci. **35**, 273–282 (2011).

Koukouvinis, P., Gavaises, M., Supponen, O., and Farhat, M., "Simulation of bubble expansion and collapse in the vicinity of a free surface," Phys. Fluids **28**, 052103 (2016a).

Koukouvinis, P., Gavaises, M., Supponen, O., and Farhat, M., "Numerical simulation of a collapsing bubble subject to gravity," Phys. Fluids **28**, 032110 (2016b).

Krishna, R., Van Baten, J. M., and Urseanu, M. I., "Scale effects on the hydrodynamics of bubble columns operating in the homogeneous flow regime," Chem. Eng. Tech. **24**(5), 451–458 (2001).

Lee, J. Y., Kim, N. S., and Ishii, M., "Flow regime identification using chaotic characteristics of two phase flow," Nucl. Eng. Des. **238**, 945–957 (2008).

Matsui, G., "Identification of flow regimes in vertical gas-liquid two-phase flow using differential pressure fluctuation," Int. J. Multiphase Flow **10**, 711–749 (1984).

Mandal, T. K., Das, G., and Das, P. K., "Prediction of rise velocity of a liquid Taylor bubble in a vertical tube," Phys. Fluids **19**, 128109 (2007).

Medjiade, W. T., Alvaro, A. R., and Schumpe, A., "Flow regime transitions in a bubble column," Chem. Eng. Sci. **170**, 263–269 (2017).

Merilo, M., Dechene, R. L., and Cichowlas, W. M., "Void fraction measurement with a rotating field conductance gauge," J. Heat Transfer **99**, 330–332 (1977).

Mi, Y., Ishii, M., and Tsoukalas, L. H., "Flow regime transition criteria for upward two-phase flow invertical tubes," Int. J. Heat Mass Transfer **27**, 723–737 (2001).

Nedeltchev, S., "New methods for flow regime identification in bubble columns and fluidized beds," Chem. Eng. Sci. **137**, 436–446 (2015).
Nedeltchev, S. and Schubert, M., "Statistical validation of the mixing length concept in bubble columns operated in the transition flow regime," J. Chem. Eng. Jpn. **48**, 107–111 (2015).
Nedeltchev, S. and Shaikh, A., "A new method for identification of the main transition velocities in multiphase reactors based on information entropy theory," Chem. Eng. Sci. **100**, 2–14 (2013).
Nydal, O. J., "An experimental investigation of slug flow," Ph.D. thesis, University of Oslo, 1991.
Omeberi-Iyari, N. K. and Azzopardi, B. F., "A study of flow patterns for gas/liquid flow in small diameter tubes," Chem. Eng. Res. Des. **85**(A2), 180–192 (2007).
Ruzicka, M. C., Drahos, J., Fialova, M., and Thomas, N. H., "Effect of bubble column dimensions on flow regime transition," Chem. Eng. Sci. **56**, 6117–6124 (2001).
Ruzicka, M. C., Drahos, J., Mena, P. C., and Teixeira, J. A., "Effect of viscosity on homogeneous-heterogeneous flow regime transition in bubble columns," Chem. Eng. J. **96**, 15–22 (2003).
Shaikh, A. and Al-Dahhan, M. H., "A review on flow regime transition in bubble columns," Int. J. Chem. React. Eng. **5**, 1542 (2007), Review R1.4.
Sharaf, D. M., Premlata, A. R., Tripathi, M. K., Karri, B., and Sahu, K. C., "Shapes and paths of an air bubble rising in quiescent liquids," Phys. Fluids **29**, 122104 (2017).
Shen, Y., Hu, L., Chen, W., and Fu, X., "Periodic and aperiodic bubbling in submerged gas-liquid jets through a microchannel," Phys. Fluids **29**, 047104 (2017).
Taitel, T., Bornea, D., and Dukler, A. E., "Modeling flow pattern transitions for steady upward gas-liquid flow in vertical tubes," AIChE J. **26**, 345–354 (1980).
Tomiyama, A., Nakahara, Y., Adachi, Y., and Hosokawa, S., "Shapes and rising velocities of single bubbles rising through an inner subchannel," J. Nucl. Sci. Technol. **40**, 136 (2003).
Tutu, N. K., "Pressure fluctuations and flow pattern recognition in vertical two-phase gas-liquid correlation," in *Proceedings of the 5th International Heat Transfer Conference*, Paper B3.9 (Japan Society of Mechanical Engineers, Tokyo, 1982), Vol. 4, pp. 120–212.
Wallis, G. B., *One Dimensional Two-Phase Flow* (McGraw-Hill Book, Co., New York, 1969).
Weisman, J., Duncan, D., Gibson, J., and Crawford, T., "Effect of fluid properties and pipe diameter on two-phase flow patterns in horizontal lines," Int. J. Multiphase Flow **5**, 437–462 (1979).
White, E. T. and Beardmore, R. H., "The velocity of rise of single cylindrical air bubbles through liquids contained in vertical tubes," Chem. Eng. Sci. **17**, 351–361 (1962).
Zukoski, E. E., "Influence of viscosity, surface tension, and inclination angle on motion of long bubbles in closed tubes," J. Fluid Mech. **25**, 821 (1966).